

*Electronic Supplementary information (ESI)*  
*accompanying*

**Towards Metal-Organic Framework based Field Effect Chemical Sensors: UiO-66-NH<sub>2</sub> for Nerve Agent Detection**

I. Stassen,<sup>a,b</sup> B. Bueken,<sup>a</sup> H. Reinsch,<sup>c</sup> J.F.M. Oudenhoven,<sup>d</sup> D. Wouters,<sup>d</sup> J. Hajek,<sup>e</sup> V. Van Speybroeck,<sup>e</sup> N. Stock,<sup>c</sup> P.M. Vereecken,<sup>a,b</sup> R. Van Schaijk,<sup>d</sup> D. De Vos<sup>a</sup> and R. Ameloot<sup>a\*</sup>

---

<sup>a</sup> Centre for Surface Chemistry and Catalysis, KU Leuven – University of Leuven, Celestijnenlaan 200F, B-3001 Leuven (Belgium). E-mail: rob.ameloot@biw.kuleuven.be

<sup>b</sup> Imec, Kapeldreef 75, B-3001 Leuven (Belgium).

<sup>c</sup> Institute of Inorganic Chemistry, Christian-Albrechts-University Kiel, Max-Eyth-Straße 2, 24118 Kiel (Germany).

<sup>d</sup> Holst Centre/imec, High Tech Campus 31, 5656 AE, Eindhoven (The Netherlands)

<sup>e</sup> Center for Molecular Modeling, Ghent University, Technologiepark 903, B-9052 Zwijnaarde (Belgium)

## **Experimental section**

### **Chemicals**

All chemicals were commercial grade and were used as received.

### **Synthesis**

UiO-66-NH<sub>2</sub> was synthesized using a scaled-up and modified literature procedure.<sup>1</sup> In a pressure-resistant screw cap bottle, 6.7 mmol ZrCl<sub>4</sub> was carefully added to a solution of 10 mmol 2-aminoterephthalic acid in 200 ml N,N-dimethylformamide. In a next step, 1 ml of HCl 37 % in water was added. The solution was ultrasonicated until complete dissolution and subsequently placed in a preheated oven at 393 K for 24 h. The yellowish precipitate was collected by centrifugation (14 min, 10 000 rpm). The precipitate was subsequently submitted to 4 washing cycles (2 x DMF, 2 x ethanol), consisting of vigorous shaking in 100 ml solvent, soaking for 12 h at 333 K and collection by centrifugation. After this procedure, the sample was dried under air at room temperature and subsequently at 100 °C in a preheated oven.

### **Characterization**

DMMP and water adsorption isotherms were measured using a Micromeritics 3Flex 3500 physisorption instrument, equipped with a thermostatic vapor source. The samples were in first degassed under vacuum at 373 K for 4 h. The uptake of DMMP was measured in the pressure range 10<sup>-6</sup> – 10<sup>-4</sup> mbar. For ease of comparison to the Kelvin probe experiments, the isotherms are plotted using the concentration of an equivalent partial pressure at atmospheric conditions (10<sup>-6</sup> bar = 1 ppm). The DMMP loaded samples (MOF<sub>DMMP-L</sub> and MOF<sub>DMMP-H</sub>) were prepared by collecting the powder from the instrument after the specific loading was reached. The reference sample went through the same procedure but was collected before exposure to DMMP. After collection, the samples were exposed to a non-dry atmosphere. ATR-FTIR spectra were recorded on a Varian 670 FTIR spectrometer coupled to a Varian 620 infrared microscope equipped with a slide-on Ge ATR tip. TPD and TGA measurements were conducted using a TA Instruments Q500 thermogravimetric analyzer (10 mg sample, 5 K min<sup>-1</sup> temperature program, oxygen purge flow). The TPD data are obtained as the first temperature derivative of the TGA signal. SEM images were recorded using a FEI XL30FEG instrument (samples were covered with 5 nm Au by sputtering).

### **Kelvin probe**

The UiO-66-NH<sub>2</sub> powder sample was suspended (10 weight %) in ethanol by ultrasonication. This solution was drop casted (10 µl) on a 2 x 2 cm<sup>2</sup> silicon substrate. After evaporation of the solvent (under air and at room temperature), the sample was dried at 363 K overnight in a preheated oven and divided in four 1 x 1 cm<sup>2</sup> samples. Kelvin probe DMMP sensing experiments were conducted using a customized KP Technology Kelvin probe cell with a gas inlet and outlet (125 cm<sup>3</sup> volume, 12 cm<sup>3</sup> piping, ca. 1000 cm<sup>3</sup> min<sup>-1</sup> gas flow). A stainless steel 3 mm probe was used. The carrier flow was generated from dry compressed air. Permeation tubes (40 and 500 ng min<sup>-1</sup>, Eco Scientific) were used for dosing of DMMP to the carrier stream. The evaporation vial with the permeation tube was kept at a constant temperature employing a thermostatic bath. The gas flow through this vial was kept constant to achieve a constant evaporation rate. Humidity was tuned by leading a part of the carrier gas through a water bubbler. Different DMMP concentrations were reached by mixing of gas streams using a computer-controlled mass flow controller assembly. Before the measurements, the sample was allowed to equilibrate in a carrier flow overnight. During the experiment the CPD was monitored while the sample was exposed to different concentrations of DMMP alternated with pure carrier gas, to monitor both adsorption and desorption responses.

### **Periodic DFT calculations**

To obtain more insight into plausible adsorption sites of the DMMP molecule in the UiO-66 type materials, both static and dynamic periodic density functional theory calculations were performed. The static periodic DFT-D3 calculations were performed with the Vienna Ab Initio Simulation Package (VASP 5.3).<sup>2-4</sup> A body centered tetragonal cell consisting of an equal amount of saturated clusters and clusters with two missing linker sites was used to estimate the adsorption interactions and energy of DMMP isolated missing linker sites. Isolation of the missing linker sites was chosen to give only minimal interactions with neighboring unit cells (figure S5). One amino group was randomly distributed for each linker (by replacing the other equivalent positions on the linker by hydrogen atoms). As water is present during the experiment, we adsorbed on the Zr Lewis acid sites four water molecules; two by physisorption and two by chemisorption by means of two hydroxyl groups. The periodic model, in which the environment of surrounding linkers and other Zr Lewis acid sites is accounted for, has previously been used to give a reliable description of the system.<sup>5,6</sup> For the simulations, the Brillouin zone was sampled by the  $\Gamma$ -point, as the UiO-66 materials have the face-centered symmetry of the  $Fm\bar{3}m$  space group. The influence of the chosen k-point mesh was previously checked.<sup>5</sup> All structures were optimized with a PBE-D3 exchange correlation functional and the projector augmented approximation.<sup>4,7</sup> A plane wave kinetic energy cut-off of 600 eV was used. The convergence criterion for the electronic self-consistent field problem was set to  $10^{-5}$  eV. The thermal corrections were performed on the basis of frequencies obtained with a full Hessian approach. As the potential energy surface is relatively flat, it is very hard to remove all imaginary frequencies as was also pointed out by De Moor *et al.*<sup>8</sup> In our case, systematically one imaginary frequency with value around  $-35\text{ cm}^{-1}$  was found, which we were unable to remove even after several geometry optimizations with slightly perturbed geometries. To get an estimate for the entropy and enthalpy, we substituted this frequency with one arbitrary frequency of  $50\text{ cm}^{-1}$  as was suggested by De Moor *et al.* Theoretical results are given in Table S1. Ab initio molecular dynamics simulations were performed with the CP2K software package<sup>9</sup> on the DFT level of theory by using the combined Gaussian Plane Wave basis sets approach.<sup>10,11</sup> The revPBE functional was chosen for its improved performance for solid-state calculations relative to the commonly used PBE functional.<sup>12</sup> The DZVP-GTH basis set and pseudopotentials<sup>13</sup> were chosen including Grimme D3 dispersion corrections.<sup>14</sup> The simulations were performed in the NPT ensemble at 300 K and 1 bar. The time step for integration of the equation of motion was set to 0.5 fs. The temperature was controlled by a chain of five Nosé-Hoover thermostats,<sup>15</sup> the pressure by an MTK barostat.<sup>16</sup>

### **X-ray structure refinement**

In order to locate DMMP-associated electron density in the UiO-66-NH<sub>2</sub> structure, high-resolution powder X-ray diffraction patterns of the native UiO-66-NH<sub>2</sub> material and MOF<sub>DMMP-L</sub> were recorded. Samples were packed in 0.5 mm glass capillaries, and mounted on a STOE Stadi MP diffractometer with focusing Ge(111) monochromator (Cu K <sub>$\alpha$ 1</sub> radiation,  $\lambda = 1.54056\text{ \AA}$ ) in Debye-Scherrer geometry (linear position sensitive Mythen detector). Data processing, including Pawley and Rietveld refinement, was performed using the TOPAS-Academic v4.3 software. Peak profiles were fitted with the Pearson VII profile function. In a first step, a structural model of UiO-66-NH<sub>2</sub> was refined against its corresponding recorded diffraction pattern. Linker C and N atom occupancies were constrained to 0.83 and 0.2075, respectively, to account for the presence of missing linker defects (corresponding to 2 missing carboxylate groups per cluster). All framework atom positions were freely refined, but soft distance restraints were applied. Residual electron density in the pores was modelled as freely refined oxygen atoms representing water molecules. Five independent water sites were found to provide the best fit. The final model provided a very good fit to the data ( $R_{wp} = 4.5\%$ ;  $GoF = 1.47$ ;  $R_{Bragg} = 1.5\%$ ). In a second step, a model for MOF<sub>DMMP-L</sub> was constructed based on the Rietveld refined model of UiO-66-NH<sub>2</sub>. Initial values for background, peak profile and zero-error parameters were drawn from the refinement of UiO-66-NH<sub>2</sub>. Since the scattering contributions of

the CH<sub>3</sub> substituents in DMMP were deemed too low to refine the position of the entire molecule, the DMMP molecule was approximated as a PO<sub>4</sub> tetrahedron. A single PO<sub>4</sub> tetrahedron was introduced into the empty framework model derived from the refined UiO-66-NH<sub>2</sub> structure and constrained as a rigid body. The position of this rigid body was allowed to refine freely, and the model was found to converge to a situation with the PO<sub>4</sub> tetrahedron on a general position located in the octahedral cavities. Residual electron density, located by Fourier mapping in the tetrahedral cavity, was subsequently refined as three independent water molecules. Finally, all framework atoms were allowed to refine freely while preserving the distance restraints defined for UiO-66-NH<sub>2</sub>. A good fit to data was obtained for the final model ( $R_{wp} = 3.3\%$ ;  $GoF = 1.44$ ;  $R_{Bragg} = 1.7\%$ ).

### Supplementary experimental results

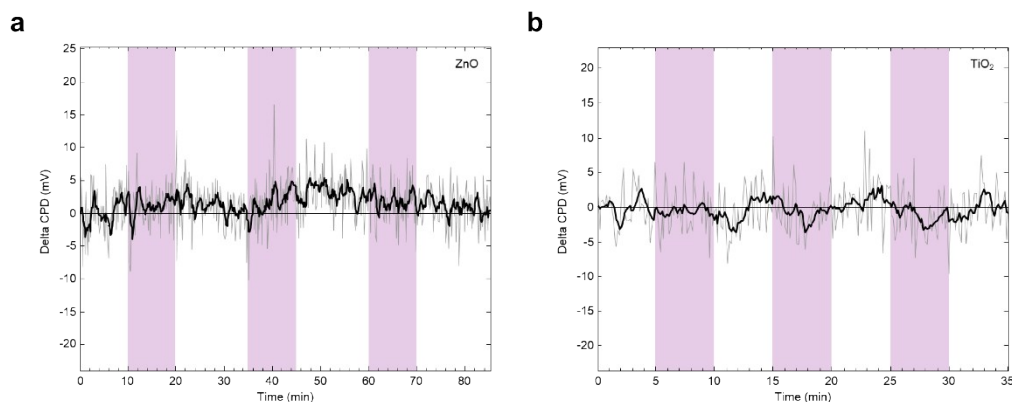


**Fig. S1.** Kelvin probe substrate control experiments. No CPD responses were observed after exposure to 80 ppb DMMP (indicated in purple) for bare silicon (not shown) and after surface functionalization with metal oxide films with anticipated active surface chemistries towards DMMP. (a) zinc oxide. (b) titanium oxide. These experiments indicate that monolayer interaction of DMMP with bare inorganic semiconductor substrates does not generate significant CPD responses.

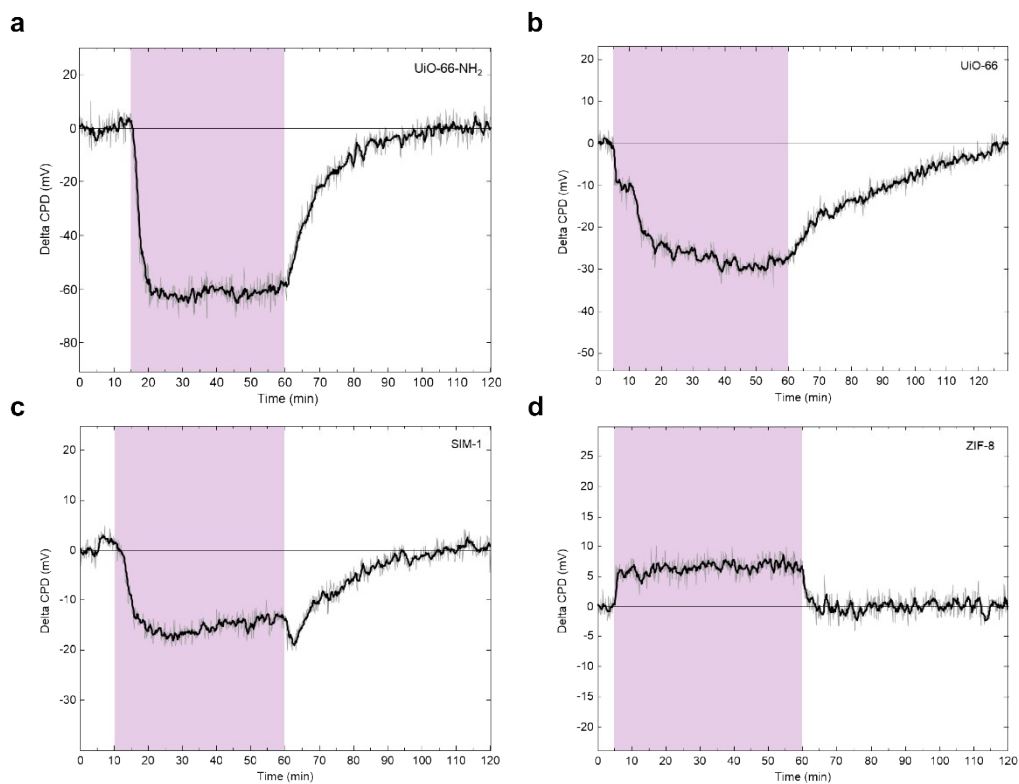


**Fig. S2.** Kelvin probe DMMP sensing screening experiments. CPD responses at 0 % RH and ca. 80 ppb DMMP (indicated in purple) using different drop casted MOF films. (a) UiO-66-NH<sub>2</sub>  $\approx$  -62 mV. (b) UiO-66  $\approx$  -28 mV. (c) SIM-1<sup>17</sup>  $\approx$  -16 mV. (d) ZIF-8<sup>18</sup>  $\approx$  5 mV. Based on these results and reports on catalytic decomposition of phosphonates, UiO-66-NH<sub>2</sub> was selected for in-depth investigation and testing at lower concentration exposures.

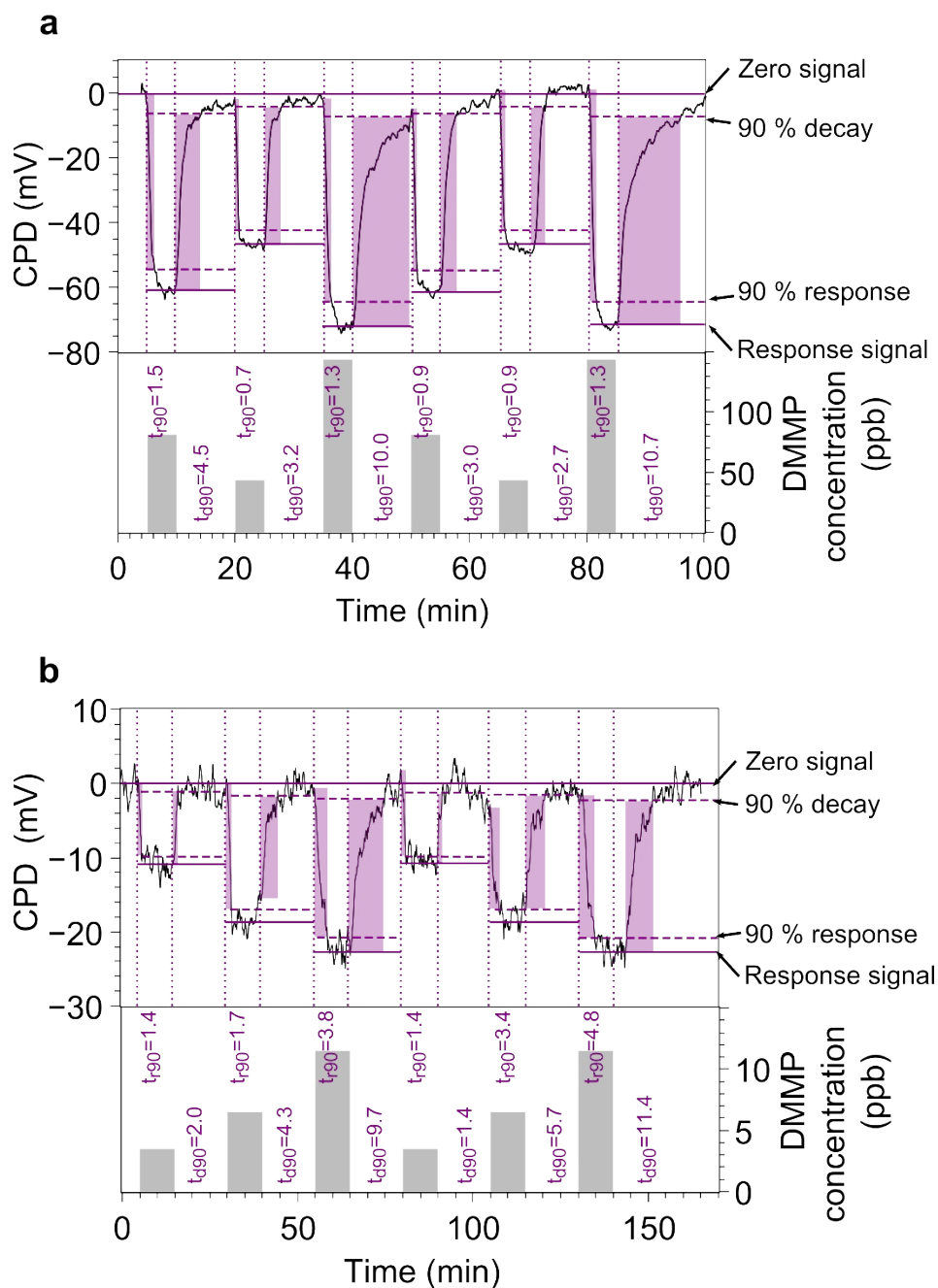


**Fig. S3.** Response  $t_{r90}$  and decay time  $t_{d90}$  analysis (time interval to reach or to drop 90 % of the signal during exposure or flushing, indicated in purple) of Kelvin probe UiO-66-NH<sub>2</sub> DMMP sensing signals in the ranges 40-150 ppb (a) and 3-15 ppb (b).

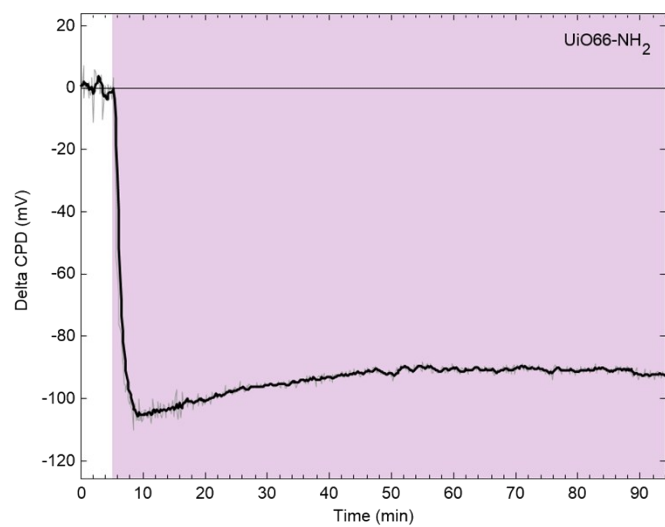


**Fig. S4.** CPD response after switching from 0 % RH air flow (white) to 50 % RH air flow (purple).

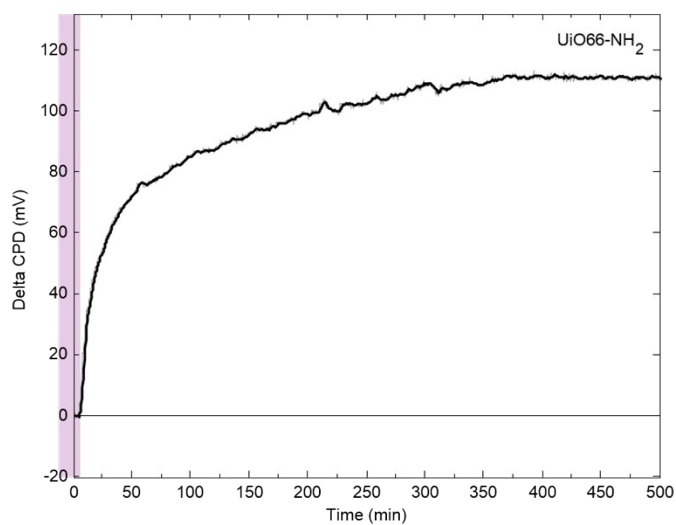


**Fig. S5.** CPD response after switching from 50 % RH air flow (purple) to 0 % RH air flow (white).

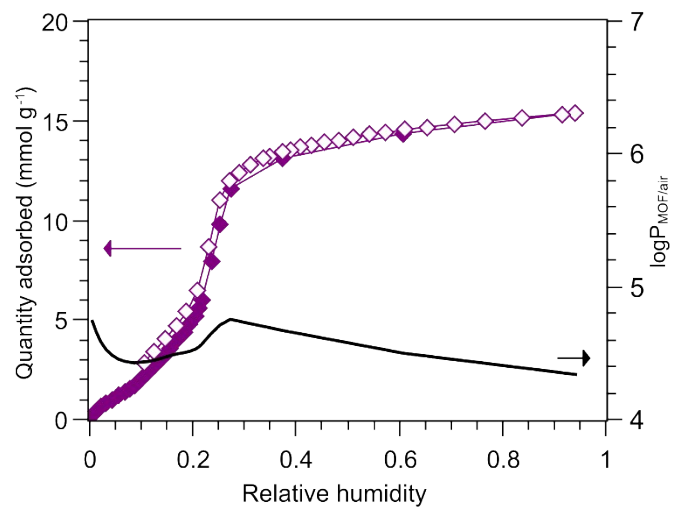


**Fig. S6.** Adsorption and desorption isotherms of water at 293 K for UiO-66-NH<sub>2</sub>. Adsorption branch, full diamonds, desorption branch empty diamonds and smooth black line, partition coefficient.

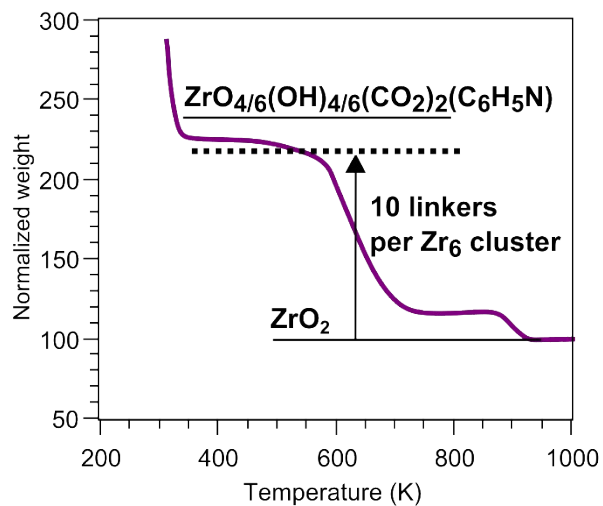


**Fig. S7.** Thermogravimetric analysis. The linker-to-cluster ratio estimated<sup>19</sup> from the organic weight loss between 423 K and 973 K is 10.5. The actual ratio is expected to be slightly lower because there is no clear separation between weight loss due to framework decomposition and weight loss due to desorption and decomposition of adsorbed guests.

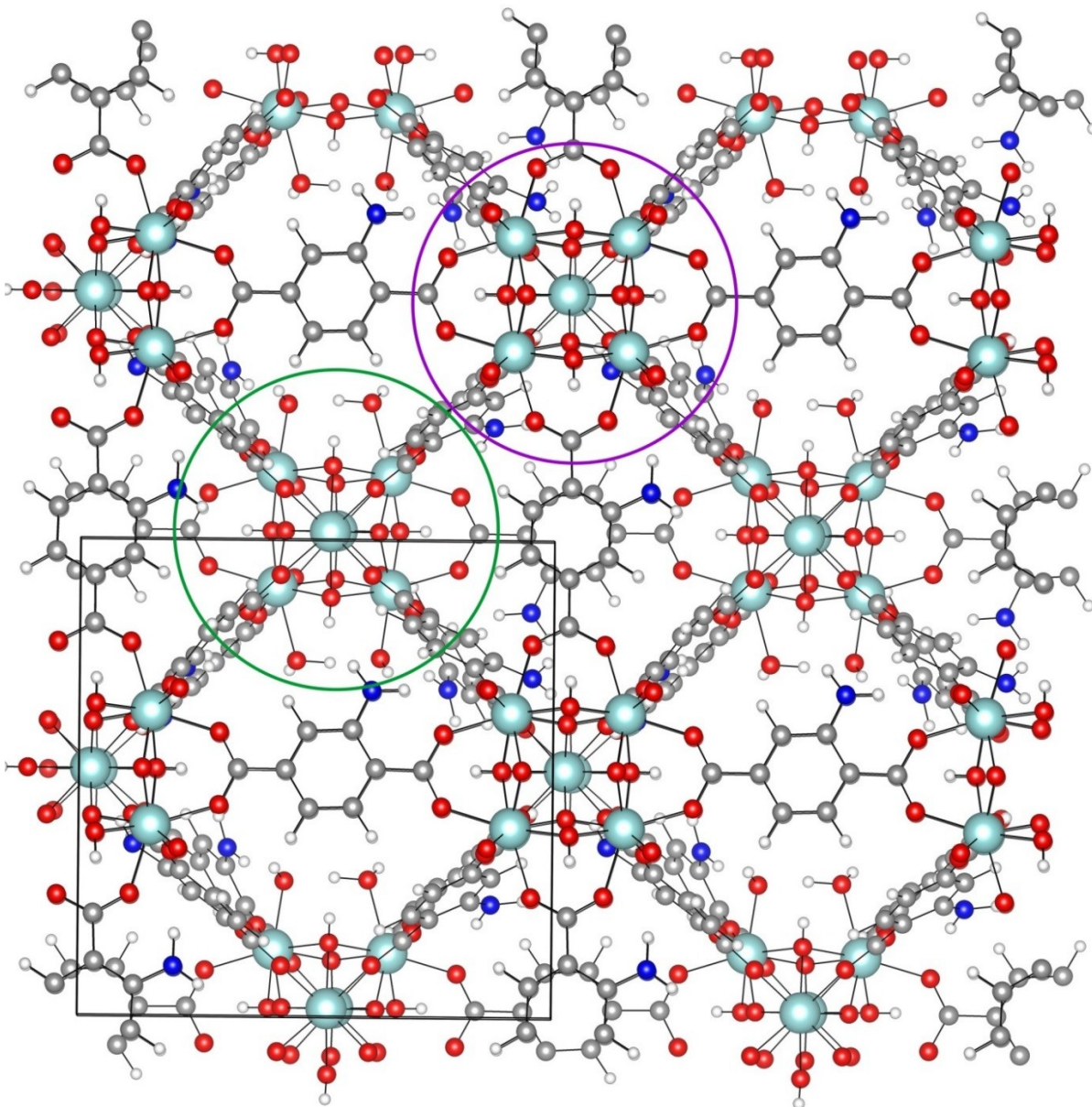


**Fig. S8:** UiO-66-NH<sub>2</sub> structure used for periodic density functional theory calculations, unit cell formula: [Zr<sub>6</sub>O<sub>4</sub>(OH)<sub>4</sub>(RCOO)<sub>6</sub>] [Zr<sub>6</sub>O<sub>6</sub>(OH)<sub>2</sub>(RCOO)<sub>5</sub>(H<sub>2</sub>O)<sub>2</sub>]. Clusters with two missing linkers defects are alternated by saturated clusters. A cluster with missing linkers is marked in green circle, while an unmodified cluster is marked in purple circle. Atom colors: Zr (light blue), O (red), C (grey), H (white), N (dark blue).

**Table S1:** Enthalpy, entropy and free energy contributions calculated at 300 K, given in kJ/mol.

	$\Delta H$	$-T\Delta S$	$\Delta G$
DMMP adsorbed in the octahedral cage	-100.1	49.7	-50.4
DMMP adsorbed in the position of missing linker	-107.6	56.5	-51.1

**Table S2:** Hirshfeld charges of the key interactions for the adsorption in the octahedral cage.

atom	Hirshfeld I-charge	atom	Hirshfeld I-charge
		O1	-0.906
N1	-0.902	N2	-0.888
C1	0.491	C4	0.495
C2	-0.356	C5	-0.363
C3	-0.280	C6	-0.282
H1	0.395	H3	0.389
H2	0.391	H4	0.385

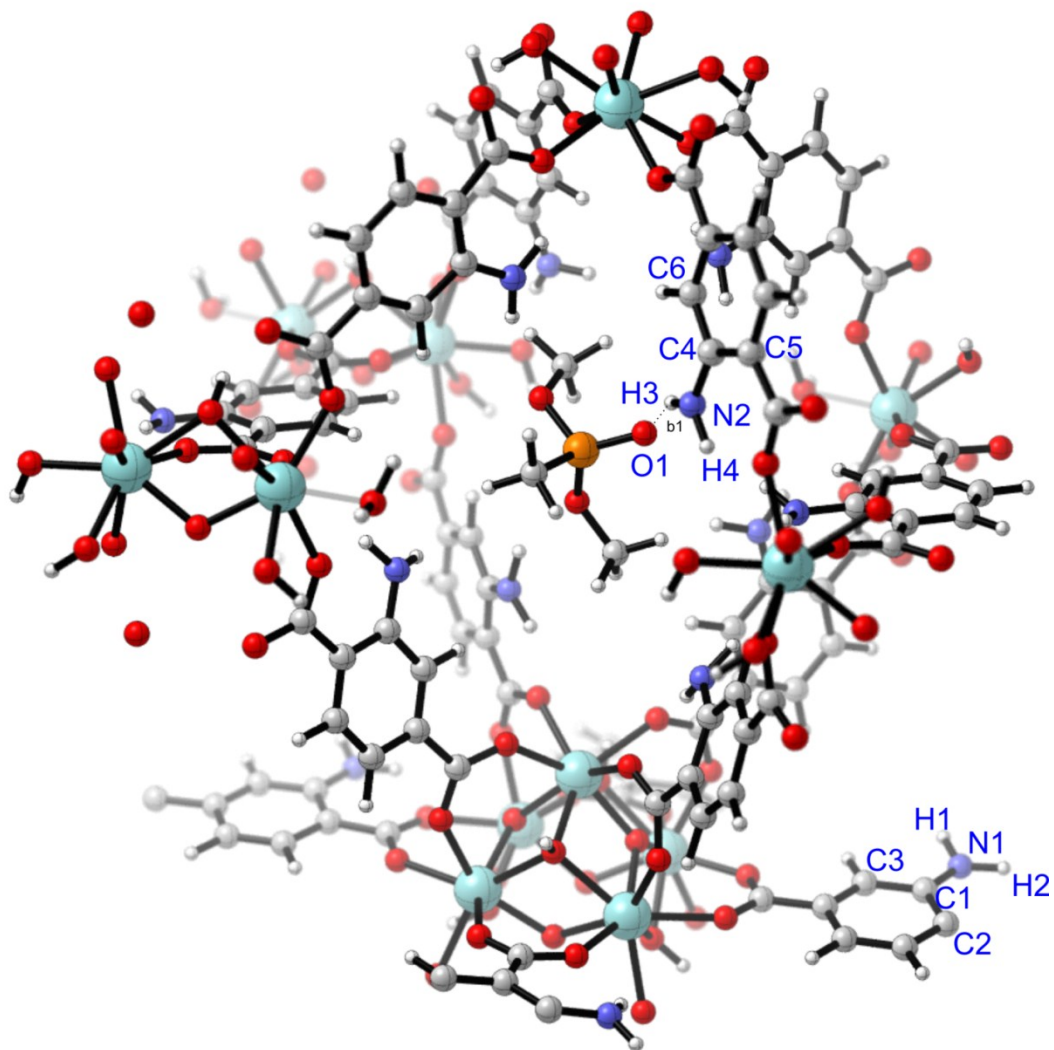


**Figure S9:** The adsorption site in the octahedral cage. The DMMP molecule is governed by the amino groups in the position of octahedral cage. Interaction b1 corresponds to the interaction which is shown in figure 3d in the manuscript. Atom colors: Zr (light blue), O (red), C (grey), H (white), N (dark blue).

**Table S3:** Hirshfeld charges of the key interactions for the adsorption in the position of the missing linker.

atom	Hirshfeld I-charge	atom	Hirshfeld I-charge
		O1	-0.904
N1	-0.899	O2	-1.097
C1	0.485	H3	0.501
C2	-0.353	H4	0.483
C3	-0.281		
H1	0.393		
H2	0.386		

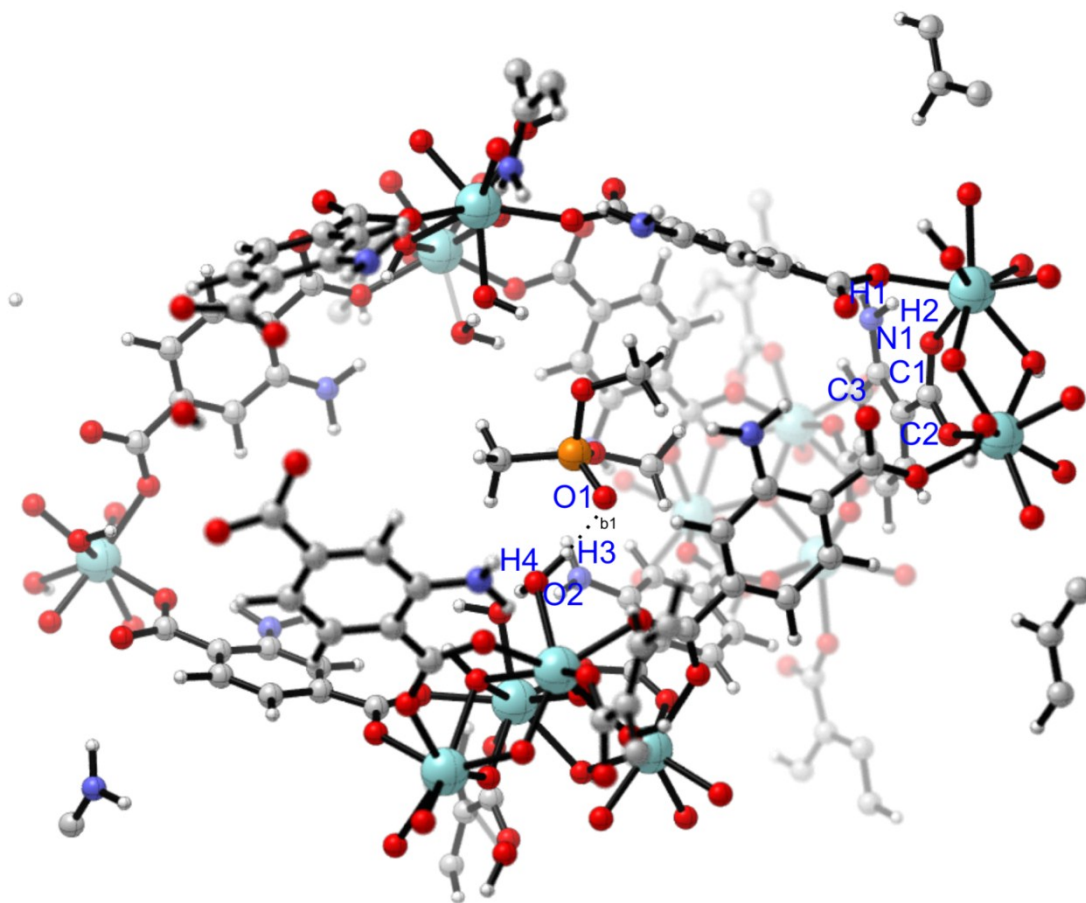


**Figure S10:** The adsorption site in the position of a missing linker defect. Interaction b1 corresponds to the interaction which is shown in figure 3d in the manuscript. Atom colors: Zr (light blue), O (red), C (grey), H (white), N (dark blue).

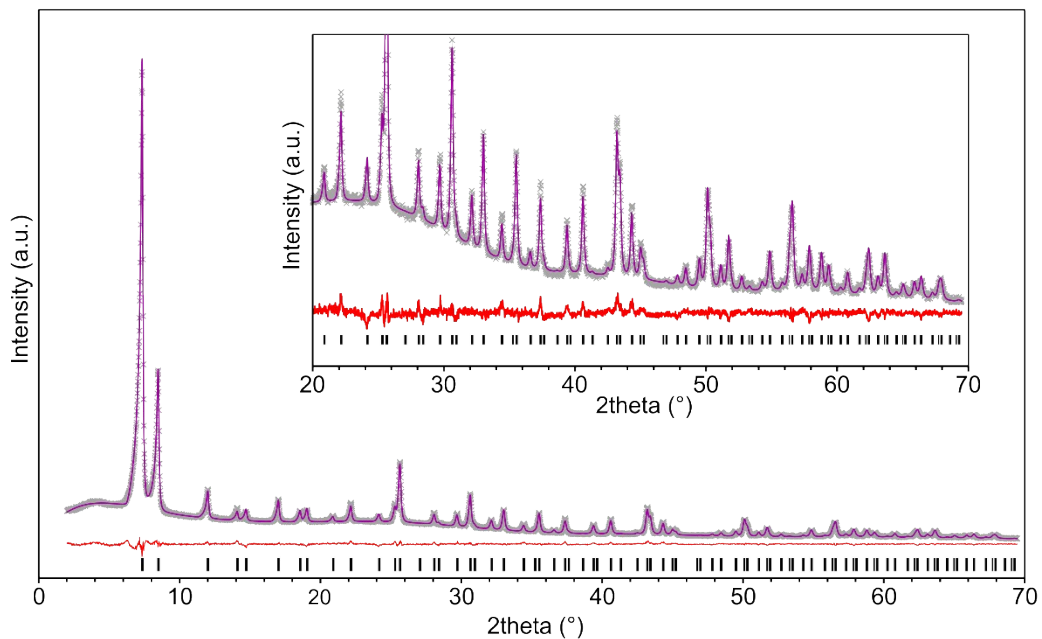


**Fig. S11.** Final plot of the Rietveld refinement of MOF<sub>DMMP-L</sub>. The inset is a detailed plot of the wide angle data. Measured data points are shown as grey crosses and the calculated fit as a purple line; the red curves indicate the difference plots. Vertical bars mark the allowed Bragg reflection positions.

**Table S4.** Crystallographic data for MOF<sub>DMMP-L</sub>.

Formula	[Zr <sub>6</sub> O <sub>4</sub> (OH) <sub>4</sub> (BDC-NH <sub>2</sub> ) <sub>5</sub> (OH <sub>n</sub> ) <sub>4</sub> ]DMMP <sub>1.44</sub>
Crystal System	Cubic
Space Group	<i>Fm</i> $\bar{3}$ <i>m</i>
a / Å	20.8179(3) Å
V / Å <sup>3</sup>	9022.1(3) Å <sup>3</sup>
Wavelength / Å	Cu K $\alpha$ <sub>1</sub>
No. Atoms	10
No. Restraints	7
R <sub>p</sub>	2.5 %
R <sub>wp</sub>	3.3 %
$\chi^2$	1.44
R <sub>Bragg</sub>	1.7 %
Formula	[Zr <sub>6</sub> O <sub>4</sub> (OH) <sub>4</sub> (BDC-NH <sub>2</sub> ) <sub>5</sub> (OH <sub>n</sub> ) <sub>4</sub> ]DMMP <sub>1.44</sub>

**Dataset S1.** Crystallographic information file for MOF<sub>DMMP-L</sub>.

```
data_
_chemical_name_mineral UiO66NH2DMMP-L
_cell_length_a 20.81786(25)
_cell_length_b 20.81786(25)
_cell_length_c 20.81786(25)
_cell_angle_alpha 90
_cell_angle_beta 90
_cell_angle_gamma 90
_cell_volume 9022.12(32)
_symmetry_space_group_name_H-M FM-3M
loop_
_atom_site_label
_atom_site_type_symbol
_atom_site_symmetry_multiplicity
_atom_site_fract_x
_atom_site_fract_y
_atom_site_fract_z
_atom_site_occupancy
_atom_site_B_iso_or_equiv
Zr1 Zr 0 0.119541(95) 0 0 1 0.200(83)
O1 O 0 0.17391(21) 0 0.09380(16) 1 2.38(17)
O2 O 0 0.05727(26) -0.05727(26) -0.05727(26) 1 2.38(17)
C1 C 0 0.26859(27) 0 0.18370(24) 0.83 8.00(49)
C2 C 0 0.15085(23) 0 0.15085(23) 0.83 8.00(49)
C3 C 0 0.20396(28) 0 0.20396(28) 0.83 8.00(49)
N4 N 0 0.30555(64) 0 0.11819(77) 0.2075 5.2(15)
O1a O 0 -0.105782 0.08623708 -0.3776882 0.03000(62) 2.38(17)
P2a P 0 -0.05733915 0.02512372 -0.3795072 0.03000(62) 8.0(36)
O3a O 0 -0.09575203 -0.03775588 -0.4050924 0.03000(62) 2.38(17)
O4a O 0 -0.02999734 0.01147522 -0.3077363 0.03000(62) 2.38(17)
O5a O 0 0.002187266 0.04055014 -0.4275014 0.03000(62) 2.38(17)
G2 O 0 0.1588(11) 0.8412(11) 0.8412(11) 0.527(21) 8.00(94)
G3 O 0 0.2906(14) 0.1845(27) 0.2906(14) 0.188(10) 8.00(94)
G4 O 0 0.3045(12) 0.3045(12) 0.3477(12) 0.2398(77) 8.00(94)
```

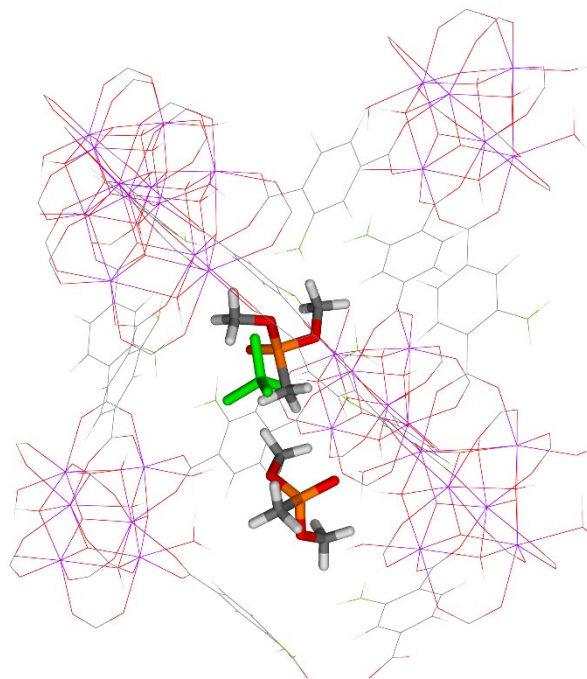


**Figure S12.** DMMP adsorption configurations modelled by DFT compared to the refined position of the tetrahedral phosphorus center of DMMP based on powder X-ray diffraction. The distance between the modelled and the refined position of the phosphorus center in the octahedral cage is 0.159 nm. Atom colors: Zr (purple), O (red), C (dark grey), H (light grey), P (orange) and N (green). The refined position is for clarity represented by a green tetrapod.

## References

- 1 M. J. Katz, Z. J. Brown, Y. J. Colón, P. W. Siu, K. A. Scheidt, R. Q. Snurr, J. T. Hupp and O. K. Farha, *Chem. Commun.*, 2013, **49**, 9449–51.
- 2 G. Kresse and J. Hafner, *Phys. Rev. B*, 1993, **47**, 558–561.
- 3 G. Kresse and J. Hafner, *Phys. Rev. B*, 1994, **49**, 14251.
- 4 G. Kresse and J. Furthmüller, *Comput. Mater. Sci.*, 1996, **6**, 15–50.
- 5 J. Hajek, M. Vandichel, B. Van de Voorde, B. Bueken, D. De Vos, M. Waroquier and V. Van Speybroeck, *J. Catal.*, 2015, **331**, 1–12.
- 6 M. Vandichel, J. Hajek, F. Vermoortele, M. Waroquier, D. E. De Vos and V. Van Speybroeck, *CrystEngComm*, 2015, **17**, 395–406.
- 7 P. E. Blöchl, *Phys. Rev. B*, 1994, **50**, 17953.
- 8 B. A. De Moor, M.-F. Reyniers and G. B. Marin, *Phys. Chem. Chem. Phys.*, 2009, **11**, 2939.
- 9 J. VandeVondele, M. Krack, F. Mohamed, M. Parrinello, T. Chassaing and J. Hutter, *Comput. Phys. Commun.*, 2005, **167**, 103–128.
- 10 B. G. Lippert and J. H. and M. Parrinello, *Mol. Phys.*, 1997, **92**, 477–488.
- 11 G. Lippert, J. Hutter and M. Parrinello, *Theor. Chem. Acc.*, 1999, **103**, 124–140.
- 12 K. Yang, J. Zheng, Y. Zhao and D. G. Truhlar, *J. Chem. Phys.*, 2010, **132**, 164117.
- 13 S. Goedecker, M. Teter and J. Hutter, *Phys. Rev. B*, 1996, **54**, 1703.
- 14 S. Grimme, J. Antony, S. Ehrlich and H. Krieg, *J. Chem. Phys.*, 2010, **132**, 154104.
- 15 D. Frenkel and B. Smit, *Understanding Molecular Simulation: From Algorithms to Applications*, Academic Press, 2001.
- 16 G. J. Martyna, D. J. Tobias and M. L. Klein, *J. Chem. Phys.*, 1994, **101**, 4177.
- 17 A. M. Marti, M. Van and K. J. Balkus, *J. Porous Mater.*, 2014.
- 18 J. Cravillon, S. Münzer, S.-J. Lohmeier, A. Feldhoff, K. Huber and M. Wiebcke, *Chem. Mater.*, 2009, **21**, 1410–1412.
- 19 L. Valenzano, B. Civalleri, S. Chavan, S. Bordiga, M. H. Nilsen, S. Jakobsen, K. P. Lillerud and C. Lamberti, *Chem. Mater.*, 2011, **23**, 1700–1718.